Alzheimer's disease-like paired helical filament assembly from truncated tau protein is independent of disulphide cross-linking

Youssra K. Al-Hilaly, Saskia J. Pollack, Devkee Vadukul, Francesca Citossi, Janet E. Rickard, Michael Simpson, John M.D. Storey, Charles R. Harrington, Claude M. Wischik, Louise C. Serpell

PII: S0022-2836(17)30444-8
DOI: doi:10.1016/j.jmb.2017.09.007
Reference: YJMBI 65501

To appear in: *Journal of Molecular Biology*

Received date: 10 June 2017
Revised date: 8 September 2017
Accepted date: 8 September 2017

Please cite this article as: Al-Hilaly, Y.K., Pollack, S.J., Vadukul, D., Citossi, F., Rickard, J.E., Simpson, M., Storey, J.M.D., Harrington, C.R., Wischik, C.M. & Serpell, L.C., Alzheimer's disease-like paired helical filament assembly from truncated tau protein is independent of disulphide cross-linking, *Journal of Molecular Biology* (2017), doi:10.1016/j.jmb.2017.09.007

Alzheimer's disease-like paired helical filament assembly from truncated tau protein is independent of disulphide cross-linking.

Youssra K Al-Hilaly[1,2], Saskia J. Pollack[1], Devkee Vadukul[1], Francesca Citossi[1], Janet E. Rickard[3], Michael Simpson[4], John M.D. Storey[4,5], Charles R. Harrington[3,5], Claude M. Wischik[3,5*], Louise C. Serpell[1*]

[1] Dementia Research group, School of Life Sciences, University of Sussex, Falmer, E Sussex, BN1 9QG

[2] College of Sciences, Chemistry Department, Al-Mustansiriyah University, Baghdad, Iraq

[3] Institute of Medical Sciences, University of Aberdeen, Aberdeen, AB25 2ZP.

[4] Department of Chemistry, University of Aberdeen, Aberdeen, AB24 3UE

[5] TauRx Therapeutics Ltd., Aberdeen, AB25 2ZP

***To whom correspondence should be addressed Louise C Serpell (L.C.Serpell@sussex.ac.uk) (+44 1273 877363) & Claude M. Wischik (cmw@taurx.com)**

Running title: Paired helical filaments composed of truncated tau

Abstract

Alzheimer's disease is characterised by the self-assembly of tau and amyloid β proteins into oligomers and fibrils. Tau protein assembles into paired helical filaments (PHFs) that constitute the neurofibrillary tangles observed in neuronal cell bodies in individuals with Alzheimer's disease. The mechanism of initiation of tau assembly into PHFs is not well understood. Here we report that a truncated 95-amino acid tau fragment (corresponding to residues 297-391 of full-length tau) assembles into PHF-like fibrils *in vitro* without the need for other additives to initiate or template the process. Using electron microscopy, circular dichroism and X-ray fibre diffraction, we have characterised the structure of the fibrils formed from truncated tau for the first time. To explore the contribution of disulphide formation to fibril formation, we have compared the assembly of tau(297-391) under reduced and non-reducing conditions and for truncated tau carrying a C322A substitution. We show that disulphide bond formation inhibits assembly and that the C322A variant rapidly forms long and highly ordered PHFs.

Highlights

- Truncated tau is a major component of paired helical filaments (PHF) in neurofibrillary tangles in Alzheimer's brain tissue and encompasses the core structure of PHF isolated from AD brain.
- Truncated tau (297-391) forms filaments that share fine structural characteristics with isolated PHF.
- Reduction of the disulphide, or replacement of Cys with Ala in truncated tau, leads to enhanced filament formation.
- Truncated unmodified tau is sufficient for the assembly of PHF found in Alzheimer's disease

Keywords: Alzheimer's disease; tau; neurofibrillary tangles; paired helical filaments; disulphide.

Introduction

Alzheimer's disease is characterised by the intracellular accumulation of insoluble neurofibrillary tangles composed of the tau protein, and the extracellular deposition of amyloid plaques. Amyloid plaques are composed predominantly of the amyloid beta peptide (Aβ) [1] whilst neurofibrillary tangles are composed of paired helical filaments (PHFs), consisting of a truncated fragment of tau protein restricted to the repeat domain [2]. Tau and Aβ peptides self-associate *in vitro* to form fibrils that share a cross-β core [3, 4]. Oligomeric species of tau have been implicated as being important in the characteristic spread of neurofibrillary degeneration throughout the brain and for the toxic effects leading to neuronal dysfunction and death [5, 6]. Several lines of evidence point to the importance of neurofibrillary tau pathology being closely associated with dementia in Alzheimer's disease (AD) and other tauopathies [7-13].

Tau protein, encoded by the *MAPT* gene, is expressed in the central nervous system as a family of six isoforms. These arise by alternative mRNA splicing and vary in length and in the content of three or four tandem repeats of 31 or 32 amino acids in the C-terminal domain [14]. Microtubules are essential in morphogenesis, cell division, and intracellular trafficking of organelles. At physiological concentrations, tau proteins stabilize microtubules as tracks for intracellular transport, but in excess they interfere with axonal transport [15]. Tau is also implicated in a number of other cellular functions, such as signal transduction, actin interaction and in the binding pericentomeric chromatin in the nucleus [16, 17]. In Alzheimer's disease and other tauopathies, tau self-assembles through the repeat domain to form PHFs and straight

filaments. Structural characterisation of PHFs isolated from AD brain tissue has revealed that the fibres display a distinct organisation of paired filaments that twist [18] or remain straight [3, 19, 20]. These filaments are also known to share the structural characteristics for amyloid, such as long unbranching filaments, high β-sheet content and they display the characteristic cross-β pattern by X-ray fibre and electron diffraction [3].

Several groups have investigated the assembly of full-length tau *in vitro* using other polyanionic molecules, such as heparin, RNA or proteoglycans, to nucleate assembly [21-23]. The tau species making up the proteolytically stable structural core of the PHF and its oligomeric precursors are derived from a mixture of fragments derived from both three- and four-repeat isoforms, but restricted to the equivalent of three repeats in length with distinct species originating from the three- and four-repeat isoforms of tau [24]. Two of the fragments from the 3- and 4-repeat isoforms terminate at the C-terminus at Glu-391, with an N-terminus at amino acid 297. The third derives from the first 3 repeats of the 4-repeat isoform and has N- and C-termini at homologous positions [24, 25]. The fragments terminating at Glu-391 can be detected specifically by the antibody mAb423 [26] which has been shown to bind to intra- and extracellular NFTs in AD brain tissue [27], [25, 28]. The features of these 95-amino acid long fragments represent the footprint of the pathological tau–tau binding interaction which locks the repeat domains into a characteristic proteolytically stable configuration and one that is abnormally phase-shifted with respect to the tubulin-binding domains in this region of tau [25]. This templated prion-like interaction propagates and is amplified through repeated proteolytic digestion cycles [2] and can be modelled within the cell milieu [29]. Full-length and truncated tau bind to the core tau fragment with an estimated K_D of 20 nM, and binding is inhibited 10-50 fold by phosphorylation [30].

Recently, a cryo-electron microscopy structure of PHFs isolated from AD brain has been

reported [31]. The core structure of these filaments is from 306 to 378 and the structure can incorporate both 3- and 4 repeat tau isoforms. The structure is an in-register parallel β-sheet formed by a β-bend and β-helix motif, linked by β -strands [31].

In this study, we have used the truncated PHF-core tau fragment, based upon the core of the PHF [18, 32] and which includes the PHF core region identified in the recently reported PHF structure [31]. The truncated fragment comprises 95-amino acids corresponding to residues 297-391 from the 441-residue tau isoform (4R2N). It is termed dGAE; where *d* identifies the N-terminal residue 297 and *GAE*, the three C-terminal residues terminating with Glu-391, as described in detail in [25]). dGAE was examined under non-reducing and reducing conditions. The 95-amino acid peptide contains a single cysteine at position 322 and we have compared the assembly of wild-type dGAE with protein in which the Cys has been substituted with Ala (dGAE-C322A). The dGAE protein self-assembles into filaments that share the characteristics of amyloid (β-sheet content, cross-β X-ray fibre diffraction pattern) and that closely resemble the PHFs isolated from AD brains. We have investigated the contribution of disulphide formation of Cys322 and show that incubation in reducing conditions or introducing a C322A substitution lead to enhanced self-assembly and the production of long and highly ordered PHFs.

Results

Assembly of truncated tau protein

Recombinant truncated dGAE tau and dGAE-C322A were expressed in bacteria and purified by ion-exchange chromatography. Purified, soluble dGAE (100 μM) was incubated in phosphate buffer, with and without 10 mM DTT. dGAE-C322A was prepared in the same manner (without DTT) and assembly into aggregates or filaments

was monitored using thioflavin-S (ThS) fluorescence at intervals up to 48 h (Figure 1). ThS has been previously shown to give an enhanced intensity when measuring tau assembly [33] and used to quantify PHFs [29]. ThS fluorescence intensity for reduced and non-reduced dGAE and dGAE-C322A increased with time indicating the gradual assembly into oligomers and filaments (Figure 1a). ThS assays are very similar to ThT and will detect assembled structures above a certain threshold (depending on concentration). As has been shown frequently, ThT and ThS begin to show a signal at time points where small oligomeric structures can be observed by electron microscopy. The elongation of the fibrils correlates with an increase in fluorescence intensity. Indeed, we detect small oligomers by TEM at the same time point as an increased ThS intensity. Each spectrum showed a similar lag-phase length; the final intensity of ThS fluorescence for dGAE-C322A after 48 h was slightly lower than for dGAE. This may reflect subtle changes in binding of ThS to the different species formed. Tyrosine fluorescence was monitored to follow changes in the environment of the tyrosine residue during assembly, and again the data suggests similar assembly rates for non-reduced dGAE and dGAE-C322A. In the presence of DTT, the tyrosine fluorescence decreased more rapidly, consistent with an alternative assembly pathway. Circular dichroism (CD) spectra showed that the dGAE transitioned from a mainly random coil conformation, with a minimum at 198 nm, to one of increasing β-sheet conformation and reduced random coil (Figure 1c). Random coil dominates the signal in the whole sample, so to investigate this further, samples were centrifuged at 20,000 x g to separate the supernatant and pellet and CD was performed on the separated samples (Figure 1c). This revealed that the suspended pellet contains protein showing a strong red-shifted β-sheet signal with a minimum at 226 nm whilst the supernatant contains protein that is predominantly random coil with a strong minimum at 197 nm. Under reducing conditions, dGAE gave a similar spectral profile to non-reduced dGAE. dGAE-C322A gave a very weak random coil signal in the supernatant fraction, suggesting a reduction

in available soluble random coil protein. The spectrum from the dGAE-C322A pellet was unusual and contained minima at 194 nm and 230 nm. To ensure that this did not arise from alignment of fibrils giving rise to linear dichroism [34], the cuvette was rotated 90°. The spectra were very similar, suggesting that this spectral difference does arise from CD. A red-shifted signal to 230 nm for β-sheet has been observed previously for elongated amyloid fibrils made from α-synuclein and may arise from extended lengths of β-structure in long fibrils [35]. To compare the assembly of dGAE, dGAE with DTT and dGAE-C322A and to complement the results of ThS and tyrosine fluorescence, the intensity of the CD signal for the supernatant only, was plotted against time (Figure S1). These results suggest that dGAE-C322A variant assembles more quickly than dGAE under reducing conditions and that both assemble more quickly than dGAE alone. Centrifugation of the samples results in difficulties in measuring protein concentrations in pellet and supernatant. Therefore, BCA assay was used to compare the concentration of protein in the pellet and supernatant for dGAE and dGAE-C322A after incubation of 48h (Figure S2). The results confirmed that less dGAE C322A remains in the supernatant compared to dGAE, supporting the view that C322A assembles more effectively than dGAE.

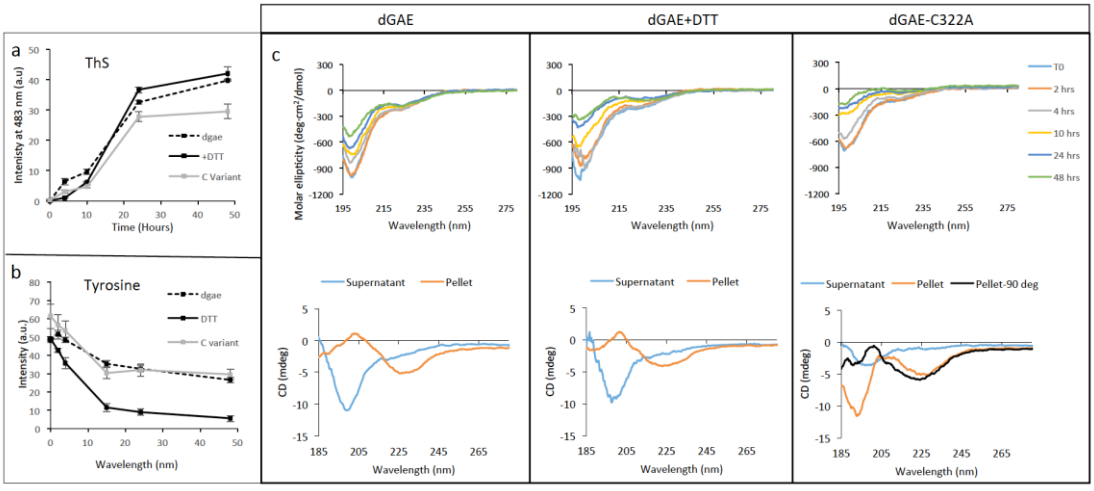

Figure 1. *Assembly of dGAE (100 μM) incubated in non-reducing and reducing conditions*

(with 10 mM DTT) and dGAE-C322A (100 μM) in PB (10 mM; pH7.4). a) Thioflavine S fluorescence assay showing assembly of all three samples over 48 h. b) Fluorescence from tyrosine decreases over time during assembly suggesting a change in the environment of the tyrosine side-chain. Data expressed as mean ± S.E. (n = 3). c) CD spectra of non-reducing and reducing dGAE and dGAE-C322A over time for the whole sample (top) and in the separated supernatant and pellet fractions (below). The whole samples show a reduction in intensity of the random coil signal (198 nm minimum) (see Figure S1) and a relative increase in intensity at 218 nm with increased time. Following separation, random coil was observed in the supernatant and β-sheet in the pellet. For the separated samples, the y axis is given in millidegrees as the unknown concentrations did not allow for conversion to molar ellipicity.

Transmission electron microscopy (TEM) was performed to compare the morphology of the dGAE samples at time points from 0 to 48 h (Figure 2). Assembly of dGAE was observed under non-reducing conditions showing the formation of small round particles which developed into slightly elongated and laterally associated fibres after 10 h incubation and which did not elongate further by 48 h. In contrast, dGAE incubated with DTT under reducing conditions formed distinct fibrillar structures by 4 h, which continued to elongate up to 48 h. dGAE-C322A formed elongated structures by 4 h, and numerous long fibrils by 24 h which associated laterally by 48 h. The ThS fluorescence assay suggested that the assembly kinetics were similar for the three protein samples (Figure 1a). However, TEM revealed significant differences in elongation and morphologies at the incubation time points examined (Figure 2).

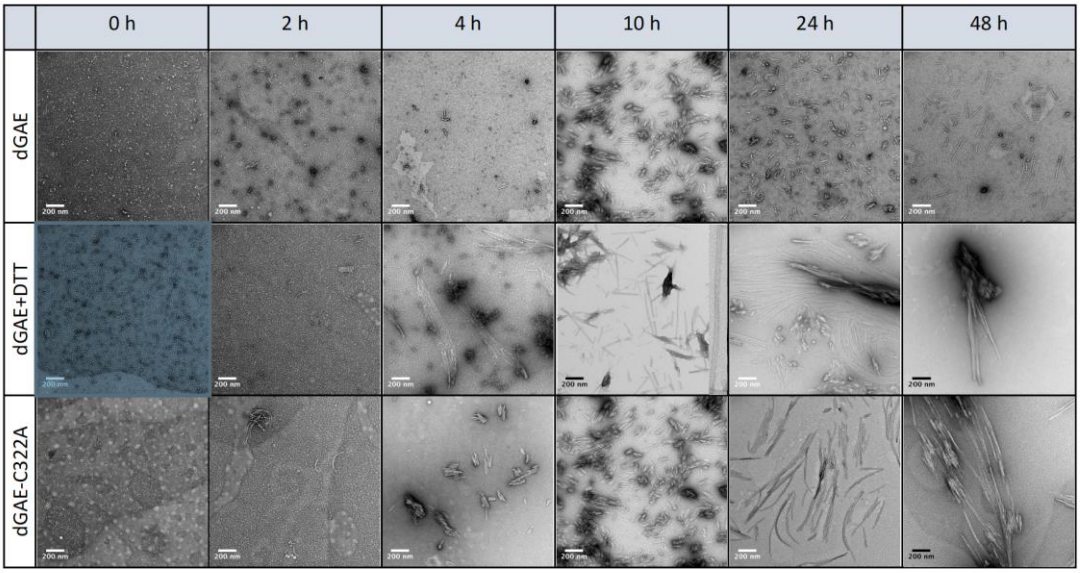

Figure 2. *TEM of dGAE (100 μM) incubated in non-reducing and reducing conditions (with 10 mM DTT) and dGAE-C322A (100 μM) in PB (10 mM; pH7.4). dGAE assembles slowly to form small elongated fibres whilst reduced dGAE forms fibrils by 10 h incubation. dGAE-C322A forms long fibrils that associate laterally by 48 h. Scale bars, 200 nm.*

SDS-PAGE was conducted on samples treated in the same way as for fluorescence assays and TEM (Figure 3). The whole sample was compared with separated supernatant and pellet fractions. dGAE ran as a doublet with mobilities of 10/12-kDa and a doublet with mobilities of 20/24-kDa (see Figure 3a insert). Since the dGAE fragment has a theoretical molecular weight of 10.27 kDa, 10 kDa is likely to represent the monomer and 20 kDa, the corresponding dimer. The 12- and 24-kDa species are likely to represent alternative folding configurations of the dGAE monomer and dimer, respectively, having retarded gel mobility. After 48 h, the intensity of the bands in the whole sample was decreased and the bands in the supernatant appeared to be similar, but with markedly decreased dimer content. The pellet was enriched selectively for the 12- and 24-kDa species as well as for some weaker bands migrating at 37-50 kDa, suggesting the presence of higher molecular weight oligomers. The data suggest that the

dGAE fragment is able to exist in two SDS-resistant conformations with different gel mobilities both as monomers and as dimers. The selective enrichment in the pellet of the 12- and 24-kDa species suggests that only one of the two conformations of dGAE is competent to aggregate into fibrils. To confirm that dGAE with DTT remained reduced following incubation for 48h, free thiols were detected using Iodoacetimide-Oregon Green 488 (IAA-OG) assay (see Supplementary information for methods). The results confirmed that the cysteine thiols remained free following incubation (Figure S3). Immunoblotting was conducted using T22, an oligomer-specific antibody [36] to gain more information about the different mobility species. T22 bound selectively with the 12- and 24-kDa species in the pellet, but not with the more abundant 10-kDa monomer present in the supernatant. T22 also labelled higher-molecular weight species at around 50 kDa in the pellet.

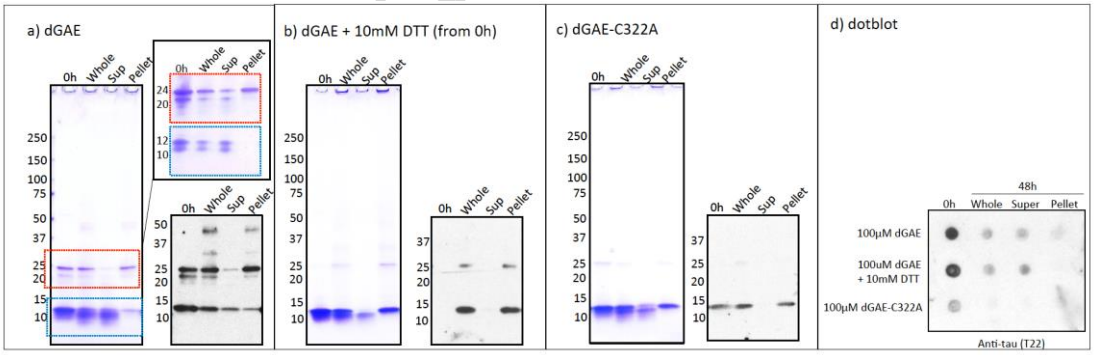

Figure 3. SDS-PAGE and immunoblot of dGAE (100 μM) *in (a) non-reducing and (b) reducing conditions (with 10 mM DTT) and (c) dGAE-C322A (100 μM). Each set of panels shows the results of Coomassie blue-stained SDS-PAGE gels (left) and immunoblot, using T22 anti-tau oligomer antibody (right), for the entire sample (whole) and the fractionated supernatant (sup) and pellet. Figure 3a shows an insert to highlight the positions of the doublet bands with reduced intensity. (d) Dot immunoblot for protein samples developed using T22* [36].

dGAE incubated under reducing conditions produced intense 10- and 12-kDa monomer

bands at 0 and 48 h, but less of the corresponding dimers than seen in the absence of DTT. Coomassie blue staining also revealed non-migrating species of very high molecular weight species in the wells. The monomer band remaining in the supernatant was substantially reduced and restricted to the species with 10-kDa mobility. The pellet contained both monomeric and dimeric species, corresponding exclusively to the 12- and 24-kDa variant. Comparison of these gels with those from non-reduced dGAE preparations suggests that the prevention of disulphide bond formation by the incubation with DTT facilitates the aggregation of the 12- and 24-kDa assembly-competent variants, leaving the 10-kDa monomer in the supernatant fraction. Also, incubation with DTT favours the formation of very high molecular weight species which are either SDS-insoluble or too large to enter the gel. Interestingly, western blotting again revealed preferential binding of T22 to the 12- and 24-kDa species, and not the 10- and 20-kDa variants seen by Coomassie staining in the whole preparation and in the supernatant fraction.

dGAE-C322A (Figure 3) showed a predominant 12-kDa monomer and a less intense 10-kDa monomer at 0 h. After 48 h, the 12-kDa species was enriched in the pellet and the 10-kDa species enriched in the supernatant. Dimer formation was less than seen either for native dGAE fragment or following incubation in DTT, and again corresponded to the 24-kDa species. Immunoblotting showed that T22 reactivity was restricted to the 12-kDa species in the pellet with no binding to the 10-kDa species predominating in the supernatant fraction at 48 h. As a control, dGAE-C322A was also separated by SDS-PAGE in the presence of DTT and no change in the mobility was observed (data not shown).

In contrast to samples separated by SDS-PAGE, dot immunoblotting showed reactivity of T22 to in all three samples at 0 h and this is likely to correspond to the 12 kDa species.

The intensity of T22 binding reduced after 48h incubation in the whole and supernatant sample and there was no binding of T22 to the pellet (Figure 3b). This suggests that the 12-kDa band is in an oligomer-like conformation and that, following filament assembly, there is occlusion of the T22 epitope(s) leading to loss of T22 binding.

Collectively, the results of ThS, Tyrosine fluoresence, TEM and SDS PAGE show that Cys-322 is unnecessary for filament assembly and that reduction of disulphide bonds, or substitution of Cys with Ala, promotes assembly to form longer and larger fibrillar structures which sediment at low speed and that these are composed predominantly of the 12-kDa variant. Furthermore, the formation of a dimer in reducing conditions is suggestive of an alternative SDS-insoluble bond being formed in dGAE [37]. One possibility is the formation of dityrosine, which remains stable in reducing conditions [38].

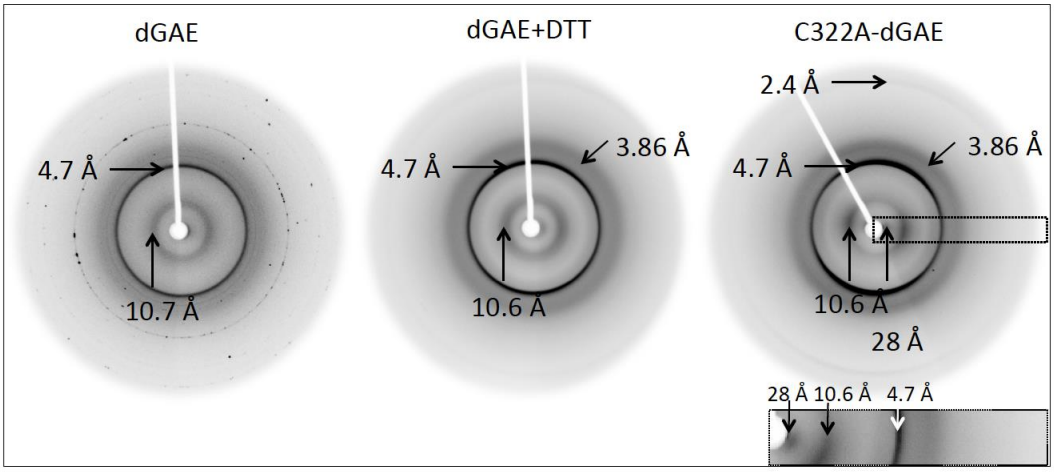

Figure 4. X-ray fibre diffraction patterns from partially aligned fibrils*. dGAE (100 μM) incubated in non-reducing and reducing conditions (with 10 mM DTT) and dGAE-C322A (100 μM) in PB (10 mM; pH7.4) washed in milliQ water before alignment. The insert highlights the diffraction signals for dGAE-C322A to show the position of 28 Å equatorial signal.*

X-ray fibre diffraction was performed for fibrils formed after 48 h incubation and revealed that all three proteins were able to form cross-β structures characteristic of amyloid fibrils (Figure 4). The diffraction patterns shared a sharp, strong 4.7 Å and a 10 Å reflection, although the pattern from dGAE was poorly aligned due to the short fibrous structures formed. However, the diffraction pattern from dGAE-C322A showed a well-aligned fibre diffraction pattern with clear 4.7 Å reflection on the meridian and 9.5 Å reflection on the equator. A low-angle diffraction signal close to the backstop was also observed at approximately 28 Å, which may arise from ordered packing of the filaments (Figure 4 insert). The patterns collected from the three fibre samples were very similar, and no obvious differences can be inferred from the patterns.

At 100 μM, dGAE forms only relatively short fibrillar structures even after incubation of up to 48 h. To investigate whether there is a concentration dependent effect leading to different fibril morphologies, dGAE was incubated at increasing concentrations from 100 μM to 400 μM.

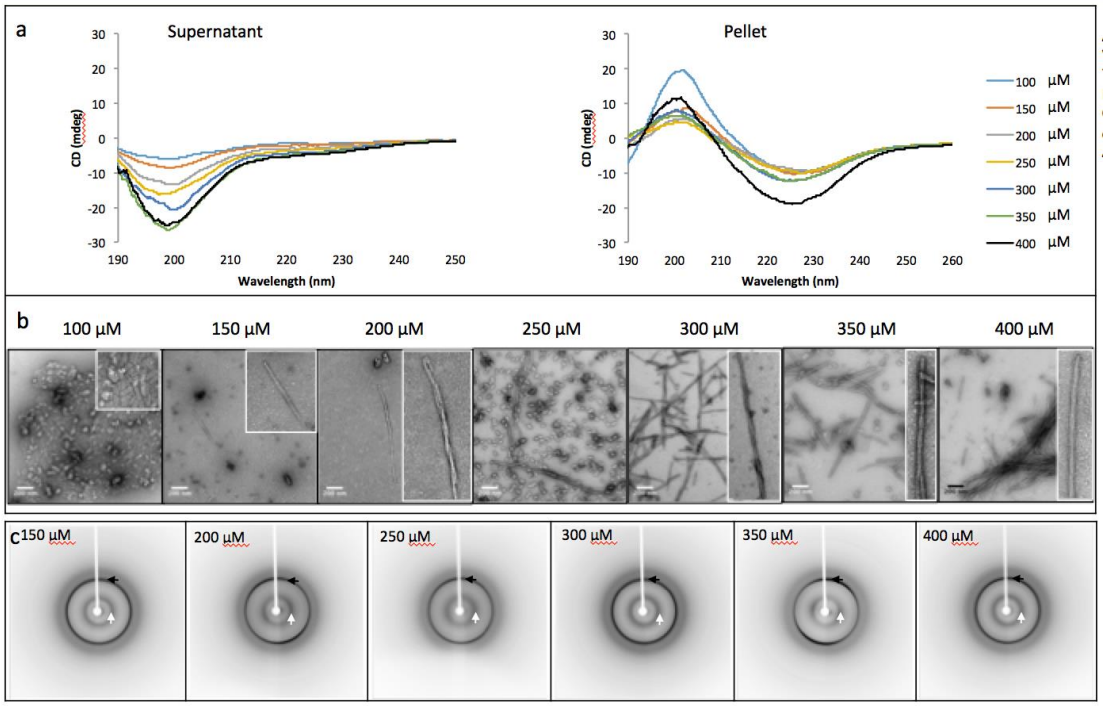

Figure 5. Characterisation of dGAE fibrils. *Fibrils were formed using different starting concentrations of protein, as indicated, and incubated at 37 °C with agitation (700 rpm) for 48 h in PB (10 mM; pH7.4). a) Comparison between the CD spectra of supernatant and pellet fractions for each concentration of dGAE. The y axis is given in millidegrees as the concentrations did not allow for conversion to molar ellipicity. The intensity at 198 nm increased with increasing concentration (see Figure S4). b) dGAE fibril morphologies by TEM. Scale bars, 200 µm (increased magnification panels included to highlight morphologies). c) X-ray fibre diffraction patterns from partially aligned filament samples formed by dGAE, at the starting concentration indicated, showing the classic "cross-β" pattern. (4.7 Å meridional is labelled with black arrow and 10-11 Å equatorial, with white arrow). Fibre axis is approximately vertical for all diffraction patterns.*

CD was used to examine the secondary structures of the dGAE at different concentrations in the separated supernatant and pellet fractions. The CD spectra of the supernatant indicated the presence of random coil structure and signal intensities at -198 nm increased with concentration (Figure S4) suggesting that a proportion of

protein remains in solution. However, the CD spectra of dGAE pellet from different starting concentrations varied considerably. All spectra were consistent with a β-sheet conformation, but the positions of the minima differed slightly, probably reflecting differences in the super-secondary structural content of the filamentous structures in the pellet (Figure 5a). ThS fluorescence was measured over 24 h and assembly rates for dGAE at low and high concentrations were compared. The findings suggest that the elongation rate increased with increased starting protein concentration (Figure S5). TEM analysis showed changes in the lateral association and twisting of the filaments. Longer fibrils were observed at 250 μM concentration, and at 300 μM, only long fibrils were observed whilst the smaller elongated particles were absent. At the highest concentration of dGAE tested (400 μM), highly ordered filaments with a clearly paired arrangement and a regular twist were observed (Figure 5b). The mean (±SD) width was 16.18 ±1.59 nm and 7.61±1.24 nm with an approximate periodicity of 73.3 ± 4.37 nm (distributions shown in Figure S6).

In order to investigate whether the molecular architecture of the filaments was dependent on concentration, X-ray fibre diffraction data were collected from all fibre samples prepared over a range of concentrations. Partially aligned fibre samples all exhibited characteristic cross-β diffraction signals (Figure 5c; white and black arrows). The patterns were very similar to one another with some small differences in alignment of the meridional and equatorial diffraction signals. TEM reveals differences in lateral packing and length but X-ray fibre diffraction reveals that the core structures were similar in all samples and consistent with the classical cross-β structure within the protofilaments core [39].

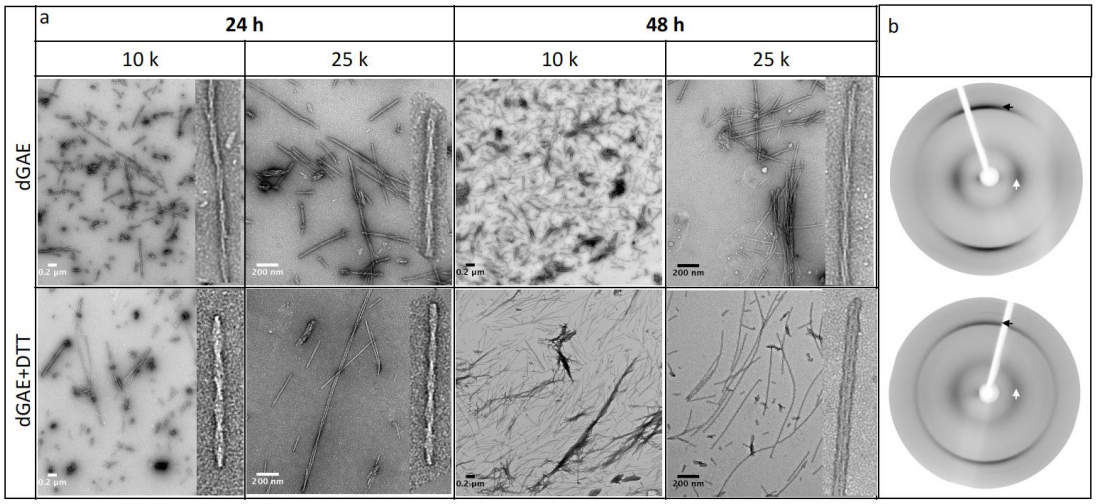

Figure 6. TEM and X-ray fibre diffraction of non-reduced and reduced dGAE at 400 µM. *a) Electron micrographs showing the twisted features of the dGAE filaments after incubation of 24 and 48 h, each shown at 10k and 25k magnification. Scale bars, 200 nm with selected inserts showing 4x magnification. b) Diffraction pattern obtained from dGAE (400 µM) without and with DTT.*

TEM and X-ray fibre diffraction were used to explore further whether there are any structural differences between dGAE incubated in non-reducing and reducing conditions at high concentrations (400 µM) (Figure 6). TEM showed that dGAE under both conditions forms paired-helical filaments that have a helical periodicity of around 80 nm. This is similar to the helical periodicity observed for PHF isolated from AD tissue [18, 32] [40, 41]. The truncated protein was able to form straight, paired filaments as well, although these were less common than the PHF morphology (approximately 10:90 ratio of SF to PHF) (see Figure S7). Straight filaments extracted from AD brain tissue constitute 5% of filaments [42]. X-ray fibre diffraction data showed the expected cross-β diffraction signals, but alignment was insufficient for further analysis. This is likely to be due to the very long filaments tangling and preventing good fibre orientation. However, the patterns show no evidence of any obvious differences between samples incubated with or without DTT.

Further analysis of the morphologies found in non-reduced and reduced dGAE samples are shown in Figure 7. Non-reduced dGAE formed a majority of PHFs with a helical repeat of 73.3 ± 4.37 nm, whilst reduced dGAE formed PHFs with a helical repeat of 65.0 ± 6.9 nm and diameters of 17.8±1.19 nm (wide) and 10.09±2.42 nm (narrow). Occasionally, wider filaments were observed with a diameter of 20 nm, which appeared to be composed of more than one pair of filaments twisted together (Figure 7). Fewer filaments with longer repeats of 83 nm were also observed. Overall, although the two samples contained a range of different species, there was no strong evidence to suggest that the structures were different when dGAE was incubated under non-reducing or reducing conditions. dGAE-C322A formed twisted ribbons consisting mostly of two protofilaments and with variable repeat lengths 392.5±32.9 nm and occasionally, single protofilaments were observed (see Figure 7).

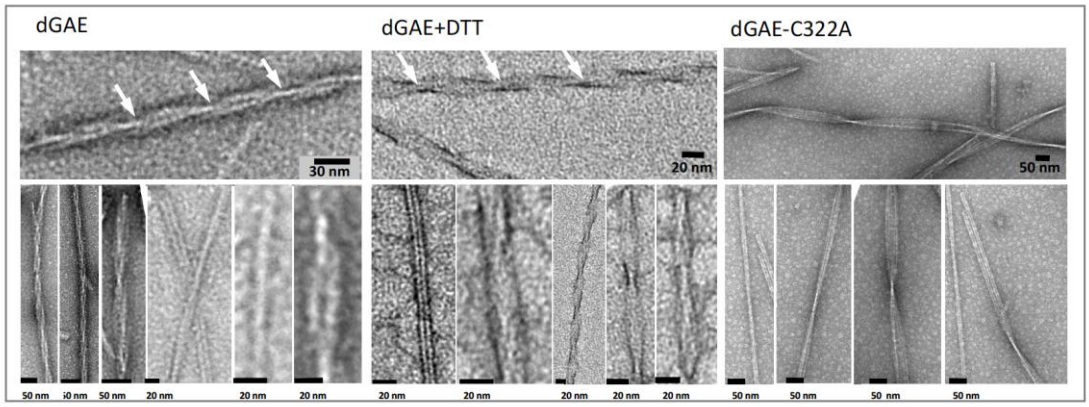

Figure 7. Electron micrographs showing the detailed morphology of the dGAE assembled under non-reducing conditions, reducing conditions (400 μM) and dGAE-C322A (100 μM). *Each condition yields paired helical filaments and some straight filaments. There is very little difference between the morphology of dGAE assembled under non-reducing and reducing conditions, whereas dGAE-C322A formed twisted ribbons consisting of paired protofilaments. Scale bars shown in nm.*

Discussion

In this study, we have shown that a truncated form of tau corresponding to a 95-amino acid region of the C-terminal domain (dGAE) is able to form filaments at physiological pH in the absence of any additives and that these closely resemble the PHFs found in neurofibrillary tangles in AD brain tissue. The dGAE fragment matches two of the species making up the structural core of the PHFs isolated from AD brain tissues [2]. Using a range of biophysical and structural approaches, we have shown that dGAE assembles in a concentration-dependent manner, with increasing β-sheet content and sharing the cross-β structure characteristic of all amyloid fibrils. Interestingly, small variations in the concentration of the protein leads to changes in the macromolecular appearance of the fibrils based upon electron microscopy observations and CD spectra. This highlights that very minor differences can have a large effect on the packing and overall morphology of filaments. Indeed, it has been shown that tau forms different filament morphologies when isolated from brain from different tauopathies, giving rise to different structural "strains" [40]. However, X-ray fibre diffraction indicated that the core cross-β structure was unaffected by these variations in macromolecular assembly.

We report that the assembly of the truncated core-tau fragment was enhanced by reducing conditions and the protein was able to form longer fibrils at the same concentration. To further explore the contribution of disulphide bond formation, we examined the assembly of dGAE-C322A and found that a species lacking any cysteine residues assembles rapidly and forms long, twisted filaments. The role for disulphide links in assembly has previously remained unclear as it has been impossible to study the effect of disulphide links on assembly in the absence of polyanionic additives, such as heparin, using full-length recombinant tau preparations [43]. We reveal that tau is able to form two types of dimer, one cysteine dependent and the other, cysteine independent. Full-length tau in COS cells has been previously shown to form cysteine dependent and

independent dimers. Variants of full-length tau (C291A/C322A) that do not contain cysteines are able to form fibrils [43]. Furukawa argued that the morphologies of filaments assembled from full-length tau can be determined by disulphide status and thioflavine T fluorescence and that disulphide-linked tau assembled more readily [44]. However, electron microscopy showed that the filaments formed with disulphide bonds were shorter than those formed in the presence of DTT, similar to our findings. The K18 fragment (a different truncated four-repeat tau fragment; tau244-372) is able to form an intra-molecular disulphide-linked monomer which is not assembly-competent [45].

Our studies suggest that a truncated tau fragment corresponding to that found in the proteolytically stable core of the PHF exists in two alternative monomeric isoforms, one with a gel mobility of 10 kDa corresponding to the theoretical molecular weight of the fragment and a corresponding dimer of 20 kDa. The second has a gel mobility corresponding to 12 kDa and a corresponding dimer of 24 kDa. Exactly the same doublet was seen in the protein extracts from the PHF-core which first permitted the identification of a truncated tau protein fragment as a structural constituent of the PHFs formed in AD [2]. The formation of the 12-kDa variant does not depend on disulphide cross-links, since it can form in the presence of an excess of DTT and also if there is a C322A substitution to produce a species lacking any cysteine residues.

The formation of the 20-kDa dimer was seen only in preparations favourable to disulphide bridge formation using native preparations of the dGAE fragment. Furthermore, the 10- and 20-kDa forms are enriched in the residual supernatant fraction left after filament assembly, whereas the 12- and 24-kDa forms are enriched selectively from the preparations of large aggregates isolated from slow-speed pellets. Conditions that inhibit filament assembly at low concentration (native dGAE at 100 μM), with formation of elongated spherical particles and short fibres at low concentration

(100 μM), are also conditions favouring the formation of the 20-kDa dimer. The addition of a reducing agent (DTT) to the assembly solution results in the ability of the short, fibrillar dGAE structures to elongate to form long twisted fibrils. Furthermore, preventing the formation of disulphide bonds by replacing the only Cys residue in dGAE with Ala leads to the rapid formation of very long fibres. Increasing dGAE concentration leads to formation of long twisted fibrils, suggesting that at sufficiently high concentration species with disulphide crosslinks no longer affect the elongation step and that it is possible to overcome the inhibition associated with formation of disulphide dimers. We suggest that, at high concentration, the nucleation process is faster than when the protein contains disulphide bonds. Since there are no obvious differences in morphology or structure of the filaments forming from native dGAE at high concentration and those forming in conditions which prevent the formation of disulphide bonds, it is likely that there is a common assembly-competent precursor conformation and that the resulting PHFs do not contain any significant amounts of disulphide-linked dGAE. We hypothesise that formation of assembly-incompetent dimers via disulphide linkages compete at the binding sites required for filament assembly thereby limiting their extent. From this interpretation, conditions unfavourable to disulphide bridge formation would facilitate the formation of the assembly-competent variant and prevent other binding interactions with assembly-incompetent dimers which impede the formation of long PHF-like filaments (Figure 8).

Our findings are consistent with the view that disulphide bond formation impedes PHF assembly. It has been shown that intramolecular disulphide bond formation stabilises aggregation-prone tau peptides in conformations inconsistent with the formation of cross-β-structure [45]. Our findings are therefore at odds with the proposal that disulphide-linked dimer formation is a critical step in the pathological aggregation of tau protein in AD [44, 46-48]. It is also at odds with the proposal that the tau aggregation

inhibitor methylthioninium chloride (MTC) acts by preventing disulphide bridge formation [49, 50]. Our data imply that if MTC were indeed able to impede cysteine cross-linking, it would have the effect of enhancing filament formation, which is not the case in cell-free or cell-based models or in disaggregation of PHFs isolated from AD brain tissue [29, 51]. Further studies aiming to elucidate the correct mechanism of action of MTC are in progress.

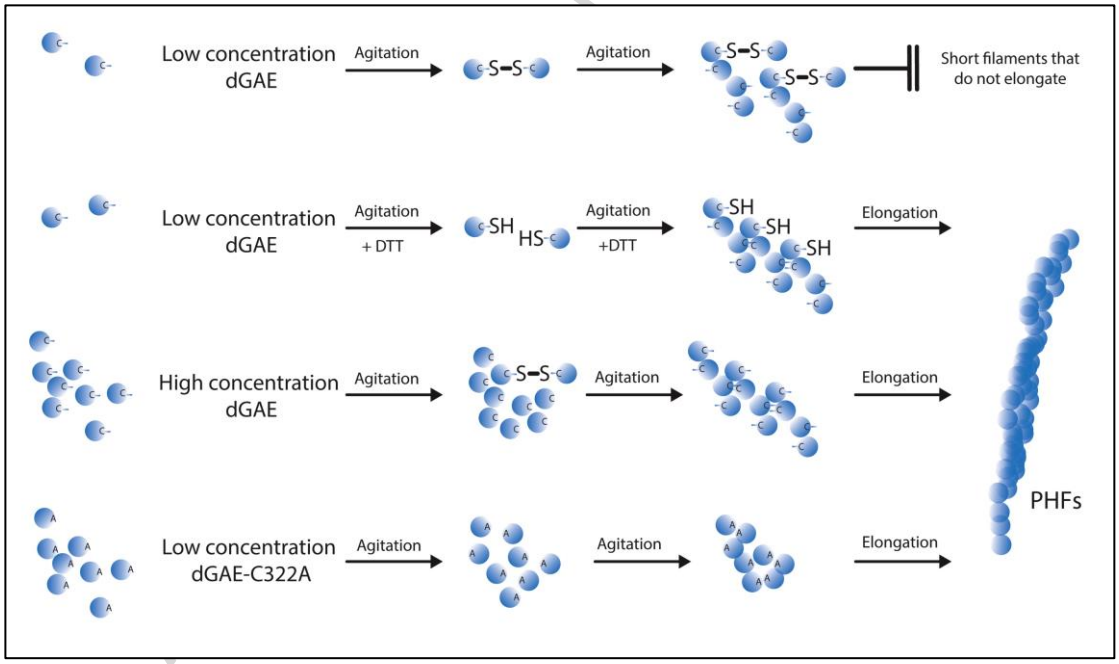

Figure 8. Schematic showing the role for disulphide bonding in assembly. *The initial dGAE solution contains monomers. At low concentration, the dGAE protein is able to form disulphide-linked dimers and with agitation, to elongate to form short filaments which cannot elongate further. This prevention of elongation can be overcome by the addition of DTT, which prevents formation of disulphide bonds and leads to the formation of an assembly competent intermediate that can elongate to form long PHFs. At high concentration of dGAE in non-reducing conditions, there is competition between formation*

of assembly competent and incompetent forms and long filaments can be formed. dGAE-C322A is unable to form disulphide bonds and is able to assemble rapidly to form long PHF.

Overall, our results show that the dGAE fragment is able to form two different species in solution under non-reducing conditions, an assembly-competent form and an assembly-incompetent form. It is striking that the 12/24-kDa variant is simultaneously enriched in the pellet and depleted from the supernatant after 48 h incubation in conditions which reduce disulphide bridge formation and which also enhance the formation of long fibres which closely resemble PHFs isolated from AD brain tissue [18, 31, 32] . It is also striking that it is the same variant which is preferentially recognised by the oligomer-specific antibody T22. Our results suggest, therefore, that there exists a specific conformation present in the 12-kDa variant, which makes it immunologically distinct from the alternative form which migrates at 10-kDa. Filaments assembled from the 12-kDa species have the same detailed morphological features as native PHFs isolated from AD brain tissue, including the characteristic longitudinal features in which four strands alternate with three-strands in the twisted ribbon configuration, and showing only four strands in the flattened ribbon configuration. These features reflect the presence of the repeating C-shaped first identified in the native PHF core [18, 32] and found also to be the repeating subunit of straight filaments [42]. It has been reported recently that the C-shaped subunit of the PHF core corresponds to a folded hairpin configuration of the core tau unit of the PHF matching closely the sequence of the dGAE fragment we have studied here [31]. In this structure, elucidated using cryo-EM analysis of ex-vivo PHF and SF, the tau folds into a cross- β/β -helix structure in residues 306-378 [31] (Figure S8). The structure also reveals that the position of the Cys side chain is buried between two -sheets and would not be available for disulphide linking with Cys from another molecule (Figure S8). This reinforces our findings that the disulphide linked dimer is assembly incompetent. We therefore infer from the data we have presented that the property of

assembly-competence that we have associated with the 12-kDa variant is directly linked with the hairpin conformation of the repeat domain found in the PHF core and recognised selectively by T22.

Previous studies have shown that the tau unit corresponding to the dGAE fragment has the ability to bind full-length tau with high affinity and to template the reproduction of the core unit with loss of proteolytically susceptible domains outside the repeat domain in the presence of proteases [51]. The stable core of the PHF has a β-sheet structure [3] whilst the fuzzy coat is thought be composed of unstructured protein chains [52] from the N- and C-terminal extensions of the molecule. Although there is considerable heterogeneity in the morphology of the filaments formed, which we have shown to depend on duration of incubation and concentration, the diffraction patterns of the different forms suggests a common underlying β-sheet molecular architecture.

We hypothesise on the basis of these results that underlying β-sheet architecture is inherent to and located within the conformation of the assembly-competent 12-kDa species. The property of dimerization shown on SDS-PAGE is not necessarily indicative of assembly competence, and indeed it is likely that formation of the 20-kDa dimer is associated with inhibition of filament assembly. Our findings suggest that the therapeutic goal of optimising inhibitors of tau aggregation may be served best by agents which either prevent the core tau protein fragment from adopting the assembly-competent configuration, or which block the association of assembly of 12-kDa subunits into toxic oligomers and filaments.

Materials and methods

Assembly of truncated tau fibrils

Recombinant truncated tau (dGAE) and dGAE-C322A were expressed in bacteria and purified by P11 phosphocellulose chromatography as described previously [51, 53], with minor modifications. In some cases, 2-(N-morpholino)ethanesulfonic acid (MES), pH 6.25, was used instead of piperazine-N,N'-bis(ethanesulfonic acid) (PIPES) and the protein was heat treated [54] instead of DE52 ion-exchange treatment prior to P11 chromatography. Protein fractions were eluted with buffer (50 mM PIPES, pH 6.8 or 50 mM MES, pH 6.25, both supplemented with 1 mM EGTA, 5 mM EDTA, 0.2 mM $MgCl_2$, 5 mM 2-mercaptoethanol) containing 0.1-1 M KCl. The peak of protein elution was identified by protein assay (at 0.3-0.5 M KCl) and dialysed against either 80 mM PIPES buffer, pH 6.8, 1 mM EGTA, 5 mM EDTA, 0.2 mM $MgCl_2$, 5 mM 2-mercaptoethanol or phosphate buffer (10 mM; pH 7.4). Protein concentration, measured using Advanced Protein Assay Reagent (Cytoskeleton, Inc.) with bovine serum albumin as a standard, was in the range 2.7-4.9 mg/ml. The protein was diluted to 10 mM phosphate buffer, pH 7.4 at a range of concentrations (100 - 400 µM) for further analysis.

Investigating the role of disulphide bond on dGAE assembly

dGAE (100 µM) with and without DTT (10 mM) was incubated at 37 °C with agitation at 700 oscillations per min (Eppendorf thermomixer C, Epppendorf, Germany) for 48 h. dGAE-C322A (100 µM) was incubated using the same assembly conditions. The assembly process was monitored using thioflavine S (ThS) fluorescence spectroscopy, tyrosine fluorescence spectroscopy, circular dichroism spectrometry (CD), negative stain transmission electron microscopy (TEM), X-ray fibre diffraction (XRFD), SDS-PAGE and immunolabelling dot blot.

Transmission electron microscopy (TEM)

Electron microscopy grids were prepared by placing 4 µl of sample onto formvar/carbon-coated 400-mesh copper grids (Agar Scientific), blotting excess and

then washing with 4 µl of 0.22 µM filtered milliQ water. Uranyl acetate (4 µL of 2% w/v) was placed on the grid twice for one minute and then blotted and the grid allowed to air-dry. Electron micrograph images were collected using a JEOL JEM1400-Plus Transmission Electron Microscope operated at 120 kV. Images were acquired digitally with an axially mounted (2000 × 2000 pixel) Gatan Ultrascan 1000 CCD camera.

Circular dichroism (CD)

CD was performed using a Jasco Spectrometer J715 and spectra collected in triplicate at a maintained temperature of 21 °C. Protein samples (30 and 60 µl) were placed into 0.1 and 0.2 mm path length quartz cuvettes (Hellma), respectively, and scanned from 180-300 nm. Since the CD spectra were dominated by a random coil signal, samples were centrifuged at 20,000 g for 30 min to separate fibrillar structures from the mixture. CD was then determined on the supernatant and pellet fractions (40 µl) separately. CD data was converted into molar ellipticity ($deg.cm^2.dmol^{-1}$) where concentrations were known.

Tyrosine fluorescence

Spectra were collected for dGAE, dGAE with 10 mM DTT, dGAE-C322A (140 µl, 100 µM) in a 10-mm cuvette. The excitation wavelength was 280 nm and an emission scan between wavelength 290-500 nm was collected using a Varian Cary Eclipse Fluorescence Spectrophotometer. The sample compartment was set to 21 ˚C with a scan rate of 600 nm/min. The data represent three independent experiments.

Thioflavin S fluorescence.

dGAE (20 µl) was mixed with ThS (280 µl, 5 µM) in 3-(N-morpholino)propanesulfonic acid (MOPS) (20 mM, pH 6.8) and then added to a 10-mm pathlength cuvette. An emission scan between 450-600 nm was obtained. The compartment was set to 21 ˚C

with a scan rate of 600 nm/min. The average of three spectra are used for each graph.

SDS-PAGE and immunoblotting

dGAE (100 μM; with or without 10 mM DTT) and dGAE-C322A were agitated at 700 rpm, 37°C for 48 h. Aliquots of the whole assembly mixture were taken at 0 and 48 h. After 48 h agitation, the whole assembly mixture was centrifuged at 20,000 g for 30 mins at 4°C. The resulting supernatant was separated from the pellet and the pellet was suspended in an equal volume of phosphate buffer (10 mM; pH 7.4). The entire assembly mixture and the supernatant and pellet fractions were used for SDS-PAGE and immunoblotting (3 μl of each per lane). For SDS-PAGE, samples were mixed with SDS sample buffer (without reducing agent) and separated using a 4-20 % gradient Mini-Protean® TGX Precast gels (Bio-Rad) at 120 V, until the sample buffer reached the end of the gel. The gel was stained using Imperial Protein Stain (Thermo Scientific), following the manufacturer's instructions, before sealing the gel and scanning on a Canon ImageRunner Advance 6055i scanner.

For immunoblotting, the separated proteins on the gel were transferred onto Amersham™ Protran™ NC nitrocellulose membrane (0.45 μm) at 200 mA for 90 min. The membranes were blocked in 5% milk in TBS-T (0.1% Tween-20) for 1 h rocking at room temperature. The membrane was incubated with T22, an antibody that recognises oligomeric tau (ABN454, Merck Millipore), in 5% milk in TBS-T (1:1000) overnight at 4°C. The membrane was incubated in secondary HRP-conjugated goat anti-rabbit antibody in 5% dried milk in TBS-T (1:10,000) for 1 h at room temperature. The membrane was developed using Clarity™ ECL blotting substrate (Bio-Rad), following the manufacturer's instructions, and then exposed to X-ray film. The membrane was washed 5 x 10 min in TBS-T in between antibody incubations.

For the dot blot, 3 µl of the whole assembly mixture, the supernatant and pellets were blotted onto Amersham Protran NC nitrocellulose membrane (0.45 µm) and were left to air dry. The membrane was rinsed in TBS-T and then immediately blocked overnight at 4°C in 5% milk in TBS-T. The membrane was incubated with T22 (1:1000) for 1 h at room temperature, followed by secondary HRP-conjugated goat anti-rabbit antibody (1:10,000) for 1 h at room temperature. The membrane was detected using Clarity ECL blotting substrate (Bio-Rad), following the manufacturer's instructions, and then exposed to X-ray film. The membrane was washed 5 x 10 mins in TBS-T between each antibody incubation.

X-ray fibre diffraction

Samples were prepared for X-ray fibre diffraction by incubating dGAE, dGAE with DTT and dGAE-C322A (diluted in 10 mM phosphate buffer, pH 7.4) for 48 h to allow formation of fibrils at 37 °C and with agitation (700 oscillations per min). The resulting fibrils were collected by centrifugation (20,000 g), washed twice with water to remove buffer salts, and 10 µl of the sample was placed between wax-tipped capillary tubes allowed to dry overnight or dried onto a Teflon slide as described previously [55]. The partially aligned samples were mounted on a goniometer head and a diffraction pattern was collected using a Rigaku rotating anode fitted with Saturn CCD detector, using an oscillation of 0.5°. Exposure times were 30 or 60 seconds and the specimen to detector distance was 50 mm or 100 mm, respectively. Diffraction data were converted to TIFF format using Mosflm [56] and inspected using CLEARER [57]. Measurements of the diffraction signals were taken using the module within CLEARER and these were then entered into the unit cell determination module, to explore possible indexing of the diffraction signals to a unit cell.

Acknowledgements

The authors would like to thank Dr Pascale Schellenberger and Dr Julian Thorpe for valuable help with TEM. TEM work was performed at the School of Life Sciences TEM imaging centre at the University of Sussex, which is supported by the Wellcome trust and RM Phillips.
LCS is supported by Alzheimer's Society and Alzheimer's Research UK Southcoast Network.

References

[1] Selkoe DJ. The molecular pathology of Alzheimer's disease. Neuron. 1991;6:487-98.

[2] Wischik CM, Novak M, Thogersen HC, Edwards PC, Runswick MJ, Jakes R, et al. Isolation of a fragment of tau derived from the core of the paired helical filament of Alzheimer disease. Proceedings of the National Academy of Sciences of the United States of America. 1988;85:4506-10.

[3] Berriman J, Serpell LC, Oberg KA, Fink AL, Goedert M, Crowther RA. Tau filaments from human brain and from in vitro assembly of recombinant protein show cross-beta structure. Proc Natl Acad Sci USA. 2003;100:9034-8.

[4] Kirschner DA, Inouye H, Duffy LK, Sinclair A, LInd M, Selkoe DJ. Synthetic Peptide Homologous to b-Protein From Alzheimer's Disease Forms Amyloid-Like Fibrils *in vitro*. Proc Natl Acad Sci USA. 1987;84:6953-7.

[5] Sanders DW, Kaufman SK, DeVos SL, Sharma AM, Mirbaha H, Li A, et al. Distinct tau prion strains propagate in cells and mice and define different tauopathies. Neuron. 2014;82:1271-88.

[6] Clavaguera F, Bolmont T, Crowther RA, Abramowski D, Frank S, Probst A, et al. Transmission and spreading of tauopathy in transgenic mouse brain. Nat Cell Biol. 2009;11:909-13.

[7] Arriagada PV, Growdon JH, Hedley-Whyte ET, Hyman BT. Neurofibrillary tangles but not senile plaques parallel duration and severity of Alzheimer's disease. Neurology. 1992;42:631-9.

[8] Wilcock GK, Esiri MM. Plaques, tangles and dementia. A quantitative study. Journal of

the neurological sciences. 1982;56:343-56.

[9] Mukaetova-Ladinska EB, Garcia-Siera F, Hurt J, Gertz HJ, Xuereb JH, Hills R, et al. Staging of cytoskeletal and beta-amyloid changes in human isocortex reveals biphasic synaptic protein response during progression of Alzheimer's disease. The American journal of pathology. 2000;157:623-36.

[10] Maruyama M, Shimada H, Suhara T, Shinotoh H, Ji B, Maeda J, et al. Imaging of tau pathology in a tauopathy mouse model and in Alzheimer patients compared to normal controls. Neuron. 2013;79:1094-108.

[11] Brier MR, Gordon B, Friedrichsen K, McCarthy J, Stern A, Christensen J, et al. Tau and Abeta imaging, CSF measures, and cognition in Alzheimer's disease. Science translational medicine. 2016;8:338ra66.

[12] Gomperts SN, Locascio JJ, Makaretz SJ, Schultz A, Caso C, Vasdev N, et al. Tau Positron Emission Tomographic Imaging in the Lewy Body Diseases. JAMA neurology. 2016;73:1334-41.

[13] Smith R, Puschmann A, Scholl M, Ohlsson T, van Swieten J, Honer M, et al. 18F-AV-1451 tau PET imaging correlates strongly with tau neuropathology in MAPT mutation carriers. Brain : a journal of neurology. 2016;139:2372-9.

[14] Crowther T, Goedert M, Wischik CM. The repeat region of microtubule-associated protein tau forms part of the core of the paired helical filament of Alzheimer's disease. Annals of medicine. 1989;21:127-32.

[15] Buee L, Bussiere T, Buee-Scherrer V, Delacourte A, Hof PR. Tau protein isoforms, phosphorylation and role in neurodegenerative disorders. Brain research Brain research reviews. 2000;33:95-130.

[16] Bukar Maina M, Al-Hilaly YK, Serpell LC. Nuclear Tau and Its Potential Role in Alzheimer's Disease. Biomolecules. 2016;6.

[17] Mansuroglu Z, Benhelli-Mokrani H, Marcato V, Sultan A, Violet M, Chauderlier A, et al. Loss of Tau protein affects the structure, transcription and repair of neuronal

pericentromeric heterochromatin. Scientific reports. 2016;6:33047.

[18] Wischik CM, Crowther RA, Stewart M, Roth M. Subunit structure of paired helical filaments in Alzheimer's disease. The Journal of cell biology. 1985;100:1905-12.

[19] Crowther R. TAU Protein and Paired Helical Filaments of Alzheimers Disease. Current opinion in structural biology. 1993;3:202-6.

[20] Schweers O, Schonbrunn-Hanebeck E, Marx A, Mandelkow E. Structural Studies of Tau Protein and Alzheimer Paired-Helical Filaments Show No evidence for b-Struture. JBC. 1994;269:24290-7.

[21] Goedert M, Jakes R, Spillantini MG, Hasegawa M, Smith MJ, Crowther RA. Assembly of microtubule-associated protein tau into Alzheimer-like filaments induced by sulphated glycosaminoglycans. Nature. 1996;383:550-3.

[22] Perez M, Arrasate M, Montejo De Garcini E, Munoz V, Avila J. In vitro assembly of tau protein: mapping the regions involved in filament formation. Biochemistry. 2001;40:5983-91.

[23] Kampers T, Pangalos M, Geerts H, Wiech H, Mandelkow E. Assembly of paired helical filaments from mouse tau: implications for the neurofibrillary pathology in transgenic mouse models for Alzheimer's disease. FEBS letters. 1999;451:39-44.

[24] Jakes R, Novak M, Davison M, Wischik CM. Identification of 3- and 4-repeat tau isoforms within the PHF in Alzheimer's disease. The EMBO journal. 1991;10:2725-9.

[25] Novak M, Kabat J, Wischik CM. Molecular characterization of the minimal protease resistant tau unit of the Alzheimer's disease paired helical filament. The EMBO journal. 1993;12:365-70.

[26] Harrington CR, Mukaetova-Ladinska EB, Hills R, Edwards PC, Montejo de Garcini E, Novak M, et al. Measurement of distinct immunochemical presentations of tau protein in Alzheimer disease. Proceedings of the National Academy of Sciences of the United States of America. 1991;88:5842-6.

[27] Mena R, Edwards P, Perez-Olvera O, Wischik CM. Monitoring pathological assembly

of tau and beta-amyloid proteins in Alzheimer's disease. Acta neuropathologica. 1995;89:50-6.

[28] Skrabana R, Kontsek P, Mederlyova A, Iqbal K, Novak M. Folding of Alzheimer's core PHF subunit revealed by monoclonal antibody 423. FEBS letters. 2004;568:178-82.

[29] Harrington CR, Storey JM, Clunas S, Harrington KA, Horsley D, Ishaq A, et al. Cellular Models of Aggregation-dependent Template-directed Proteolysis to Characterize Tau Aggregation Inhibitors for Treatment of Alzheimer Disease. The Journal of biological chemistry. 2015;290:10862-75.

[30] Lai RY, Harrington CR, Wischik CM. Absence of a Role for Phosphorylation in the Tau Pathology of Alzheimer's Disease. Biomolecules. 2016;6.

[31] Fitzpatrick AWP, Falcon B, He S, Murzin AG, Murshudov G, Garringer HJ, et al. Cryo-EM structures of tau filaments from Alzheimer's disease. Nature. 2017;547:185-90.

[32] Crowther RA, Wischik CM. Image reconstruction of the Alzheimer paired helical filament. The EMBO journal. 1985;4:3661-5.

[33] Barghorn S, Davies P, Mandelkow E. Tau paired helical filaments from Alzheimer's disease brain and assembled in vitro are based on beta-structure in the core domain. Biochemistry. 2004;43:1694-703.

[34] Morris KL, Rodger A, Hicks MR, Debulpaep M, Schymkowitz J, Rousseau F, et al. Exploring the sequence-structure relationship for amyloid peptides. The Biochemical journal. 2013;450:275-83.

[35] Serpell LC, Berriman J, Jakes R, Goedert M, Crowther RA. Fiber diffraction of synthetic a-synuclein filaments shows amyloid-like cross-b conformation. Proc Natl Acad Sci USA. 2000;97:4897-902.

[36] Lasagna-Reeves CA, Castillo-Carranza DL, Sengupta U, Sarmiento J, Troncoso J, Jackson GR, et al. Identification of oligomers at early stages of tau aggregation in Alzheimer's disease. FASEB journal : official publication of the Federation of American Societies for Experimental Biology. 2012;26:1946-59.

[37] Reynolds MR, Berry RW, Binder LI. Site-specific nitration and oxidative dityrosine bridging of the tau protein by peroxynitrite: implications for Alzheimer's disease. Biochemistry. 2005;44:1690-700.

[38] Al-Hilaly YK, Biasetti L, Blakeman BJ, Pollack SJ, Zibaee S, Abdul-Sada A, et al. The involvement of dityrosine crosslinking in alpha-synuclein assembly and deposition in Lewy Bodies in Parkinson's disease. Scientific reports. 2016;6:39171.

[39] Sunde M, Serpell LC, Bartlam M, Fraser PE, Pepys MB, Blake CC. Common core structure of amyloid fibrils by synchrotron X-ray diffraction. Journal of molecular biology. 1997;273:729-39.

[40] Spillantini MG, Crowther RA, Goedert M. Comparison of the neurofibrillary pathology in Alzheimer's disease and familial presenile dementia with tangles. Acta neuropathologica. 1996;92:42-8.

[41] Wille H, Drewes G, Biernat J, Mandelkow EM, Mandelkow E. Alzheimer-like paired helical filaments and antiparallel dimers formed from microtubule-associated protein tau in vitro. The Journal of cell biology. 1992;118:573-84.

[42] Crowther R. REVIEW: Structural Aspects of Pathology in Alzheimers Disease. biochim & Biophys Acta. 1991;1096:1-9.

[43] Sahara N, Maeda S, Murayama M, Suzuki T, Dohmae N, Yen SH, et al. Assembly of two distinct dimers and higher-order oligomers from full-length tau. The European journal of neuroscience. 2007;25:3020-9.

[44] Furukawa Y, Kaneko K, Nukina N. Tau protein assembles into isoform- and disulfide-dependent polymorphic fibrils with distinct structural properties. The Journal of biological chemistry. 2011;286:27236-46.

[45] Walker S, Ullman O, Stultz CM. Using intramolecular disulfide bonds in tau protein to deduce structural features of aggregation-resistant conformations. The Journal of biological chemistry. 2012;287:9591-600.

[46] Schweers O, Mandelkow EM, Biernat J, Mandelkow E. Oxidation of cysteine-322 in

the repeat domain of microtubule-associated protein tau controls the in vitro assembly of paired helical filaments. Proceedings of the National Academy of Sciences of the United States of America. 1995;92:8463-7.

[47] Barghorn S, Mandelkow E. Toward a unified scheme for the aggregation of tau into Alzheimer paired helical filaments. Biochemistry. 2002;41:14885-96.

[48] Kim D, Lim S, Haque MM, Ryoo N, Hong HS, Rhim H, et al. Identification of disulfide cross-linked tau dimer responsible for tau propagation. Scientific reports. 2015;5:15231.

[49] Akoury E, Pickhardt M, Gajda M, Biernat J, Mandelkow E, Zweckstetter M. Mechanistic basis of phenothiazine-driven inhibition of Tau aggregation. Angewandte Chemie. 2013;52:3511-5.

[50] Crowe A, James MJ, Lee VM, Smith AB, 3rd, Trojanowski JQ, Ballatore C, et al. Aminothienopyridazines and methylene blue affect Tau fibrillization via cysteine oxidation. The Journal of biological chemistry. 2013;288:11024-37.

[51] Wischik CM, Edwards PC, Lai RY, Roth M, Harrington CR. Selective inhibition of Alzheimer disease-like tau aggregation by phenothiazines. Proceedings of the National Academy of Sciences of the United States of America. 1996;93:11213-8.

[52] Gellermann GP, Byrnes H, Striebinger A, Ullrich K, Mueller R, Hillen H, et al. Abeta-globulomers are formed independently of the fibril pathway. Neurobiol Dis. 2008;30:212-20.

[53] Brandt R, Kempf M, Lee G. Expression and purification of tau for in vitro studies. In: Avila J, Brandt R, Kosik KS, editors. Brain Microtubule Associated Proteins: Modifications in Disease Amsterdam: Harwood Academic Publishers; 1997. p. 245-57.

[54] Vera JC, Rivas CI, Maccioni RB. Heat-stable microtubule protein MAP-1 binds to microtubules and induces microtubule assembly. FEBS letters. 1988;232:159-62.

[55] Morris KL, Serpell LC. X-ray fibre diffraction studies of amyloid fibrils. Methods in molecular biology. 2012;849:121-35.

[56] Winn MD. An overview of the CCP4 project in protein crystallography: an example of a collaborative project. J Synchrotron Radiat. 2003;10:23-5.

[57] Makin OS, Sikorski P, Serpell LC. CLEARER: a new tool for the analysis of X-ray fibre diffraction patterns and diffraction simulation from atomic structural models. Appl Cryst. 2007;40: 966-72.

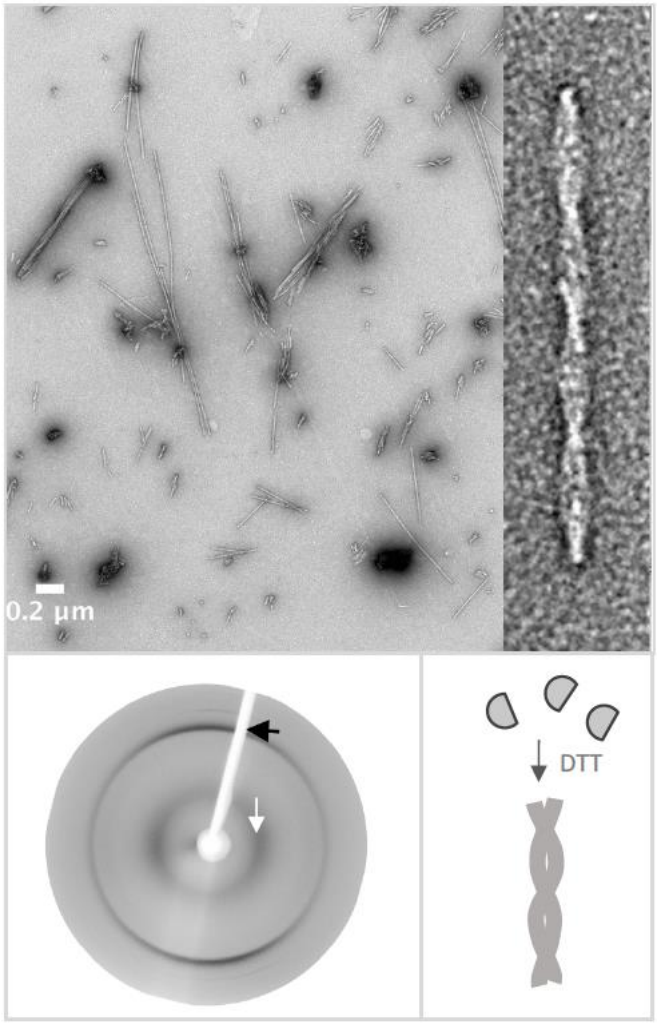

Graphical abstract

Highlights

- Truncated tau is a major component of paired helical filaments (PHF) in neurofibrillary tangles in Alzheimer's brain tissue and encompasses the core structure of PHF isolated from AD brain.
- Truncated tau (297-391) forms filaments that share fine structural characteristics with isolated PHF.
- Reduction of the disulphide, or replacement of Cys with Ala in truncated tau, leads to enhanced filament formation.
- Truncated unmodified tau is sufficient for the assembly of PHF found in Alzheimer's disease